Taylor & Francis
Taylor & Francis Group

Advanced Composite Materials

ISSN: 0924-3046 (Print) 1568-5519 (Online) Journal homepage: http://www.tandfonline.com/loi/tacm20

Impact source localization for composite structures under external dynamic loading condition

Byeong-Wook Jang, Yeon-Gwan Lee, Chun-Gon Kim & Chan-Yik Park

To cite this article: Byeong-Wook Jang, Yeon-Gwan Lee, Chun-Gon Kim & Chan-Yik Park (2015) Impact source localization for composite structures under external dynamic loading condition, Advanced Composite Materials, 24:4, 359-374, DOI: 10.1080/09243046.2014.917239

To link to this article: http://dx.doi.org/10.1080/09243046.2014.917239

Advanced Composite Materials, 2015
Vol. 24, No. 4, 359–374, http://dx.doi.org/10.1080/09243046.2014.917239

Impact source localization for composite structures under external dynamic loading condition

Byeong-Wook Jang[a]*, Yeon-Gwan Lee[b], Chun-Gon Kim[c] and Chan-Yik Park[b]

[a]*Civil Aircraft Systems Division, Korea Aerospace Research Institute, 169-84 Gwahangno, Yuseong-gu, Daejeon 305-806, Republic of Korea;* [b]*Agency for Defense Development, Yuseong P.O. Box 35, Daejeon 305-600, Republic of Korea;* [c]*Department of Aerospace Engineering, School of Mechanical, Aerospace and System Engineering, KAIST, 335 Gwahangno, Yuseong-gu, Daejeon 305-701, Republic of Korea*

(*Received 24 October 2013; accepted 18 April 2014*)

This paper suggests a real-time impact localization algorithm for a stiffened composite structure using acoustic emission signals acquired by multiplexed fiber Bragg grating (FBG) sensors. The suggested algorithm requires a database composed of premeasured impact signals at all training points to be used as reference signals. Once the FBG signals were measured from an arbitrary impact event, the root mean-squared (RMS) values were calculated between the obtained signals and all reference signals. Then, the training point that has the minimum RMS values was determined as the resultant impact location. In order to validate the applicability of this algorithm in the external environment, impact localization was performed under a dynamic loading condition. The dynamic loading condition was simulated by exciting the test article using a shaker. The results of validation tests show that the proposed algorithm could successively estimate the impact locations under a dynamic loading condition.

Keywords: impact source localization; multiplexed fiber Bragg grating sensors; high-speed fiber Bragg grating interrogator; acoustic emission; external dynamic loading condition

1. Introduction

In general, conventional metals can effectively absorb external energies due to low velocity impact over their elastic ranges by plastic deformations. Thus, the impact events can be visually identified through permanent external damage. However, composite materials have short plastic deformation ranges as well as low inter-laminar shear and transverse tensile strengths. Due to these reasons, an undetectable damage such as delamination or matrix crack easily occurs on the opposite side of the impact or inside the laminates. Such damage can degrade the mechanical properties of a structure, and thereby cause unexpected problems such as reduced life time or catastrophic failure. Moreover, internal damage cannot be easily detected by traditional non-destructive tests, and impact events such as hailstones and bird strikes may occur frequently in operation. Thus, in order to secure high reliability and safety of composite aircraft structures, an *in situ* impact monitoring system with a built-in sensor network is highly demanded.

*Corresponding author. Email: jangbw@kari.re.kr

Since 1980, numerous studies have been performed on impact localization [1–21] and damage assessment [22–25] for metallic and composite structures. As representative methods for impact source localization, the triangulation method [1,6,10,13–16] and neural network algorithm [3,5,7,12] have been widely used. However, a triangulation method using impact-generated wave speed is not adequate for anisotropic structures, because the wave speed is not constant in all directions. In order to overcome this problem, Greene et al. [1] proposed a non-linear equation for impact localization with the elimination of wave speed terms. Ciampa and Meo [13] meanwhile suggested an acoustic emission (AE) source localization algorithm without using wave speed in anisotropic materials. Baxter [14] applied Delta T source location method to an aerospace component structure with complex geometries. Also, Kundu [15] and Hajzargerbashi [16] overcame the weakness of conventional triangulation methods in anisotropic structures by optimizing the objective functions. However, although these methods provide simple tools for impact localizations, they essentially require accurate information about time-of-flight and wave speed. Because such information is hard to be accurately obtained, the applications of triangulation methods have to be limited. While a neural network algorithm provides a good solution for impact identification, there are still some limitations such as difficulty in obtaining stable neural network inputs, long training time, and so on. Other studies using dynamic strain histories [2,8,9] have yielded reliable analytical and experimental results, but they required numerous sensors and complex signal-processing methods. The time-reversal method [17–20] also has been investigated for localizing impact source and damage. In order to use the time-reversibility of acoustic waves for impact localizations, the baseline signals have to be obtained through the training procedure. They showed reliable localization results, however, a prior knowledge of acoustic waves along the target structures has to be precisely studied for high accuracy.

Impact localization methods can be classified according to the used sensor types (fiber optic sensors [1–5] and other types of sensors [6–21]). Although electrical sensors have been widely studied, there have some notable disadvantages such as susceptibility to electromagnetic interference, the use of bulky lead wires, and low sensor durability compared with fiber optic sensors. However, with optical fiber sensors, it is difficult to simultaneously detect multipoint ultrasonic signals. For efficient impact monitoring capable of detecting impact locations and damage simultaneously, AE signals of frequency exceeding 50 kHz are required. Thus, multipoint AE-sensing techniques using fiber Bragg grating (FBG) sensors have been suggested.[26–28] However, these methods have not been widely utilized in real applications due to high system cost for numerous tunable lasers [26] and the requirement of careful sensor installation methods.[27,28] Despite limitations, it is anticipated that these techniques can be applied to realize effective sensing systems in the near future.

In this study, a real-time impact localization algorithm for a composite-stiffened panel using four surface-mounted FBG sensors was suggested. Four FBG sensor heads were connected in one optical fiber line, and ultrasonic signals induced by low-velocity impact were captured by a commercial high-speed FBG interrogator (SFI-710, Fiberpro Inc., Republic of Korea). This interrogator is capable of measuring high frequency signals from up to six FBG sensors with a sampling frequency of 100 kHz.[29] First, a reference signal database composed of FBG signals at all training points was constructed. Then, by comparing the obtained signals to all reference signals, an impact location was determined. The validity of the proposed algorithm was tested under external dynamic loading condition, because most of the low-velocity impact events can be

induced in operation. From the validation tests under various excitation frequencies, the acceptance of the proposed algorithm was evaluated.

2. Experiments

2.1. Experimental setup

The composite-stiffened panel considered in this study is a mid-part of the composite wing box structure. The stiffened panel is comprised of an upper skin, a spar, and several stringers. The specimen was fabricated using a graphite/epoxy prepreg (USN 175BX, SK Chemical Co. Ltd., Republic of Korea), and the stacking sequence of the upper skin is $[\pm 45/0/45/90/-45]_s$. In order to acquire impact-generated wave signals, four FBG sensors connected in a single optical fiber line were used. Because the suitable bandwidth of FBG reflective spectrum for SFI-710 interrogation system is over 40 pm, the FBG sensors with a grating length of 5 mm were adopted. Figure 1 shows the experimental setup and boundary conditions. The FBG sensors were surface mounted on the bottom side of the upper skin, and each sensor is oriented towards the center of the section, which is thus surrounded by sensors. This FBG array was then connected to the high-speed FBG interrogator (SFI-710).

The test section is divided into three regions: Region 1, Region 2, and Region 3. Region 1 is surrounded by FBG sensors, and Region 2 is an intermediate spar-bonding region. Region 3 is the remaining region of the upper skin (not surrounded by sensors). The overall dimension is $600 \times 900\ mm^2$, and the dimensions of each region are 600×500, 600×200, and $600 \times 200\ mm^2$, respectively. The grid size for training is 50 mm, and the total number of training points is 247. The impact events were given by an

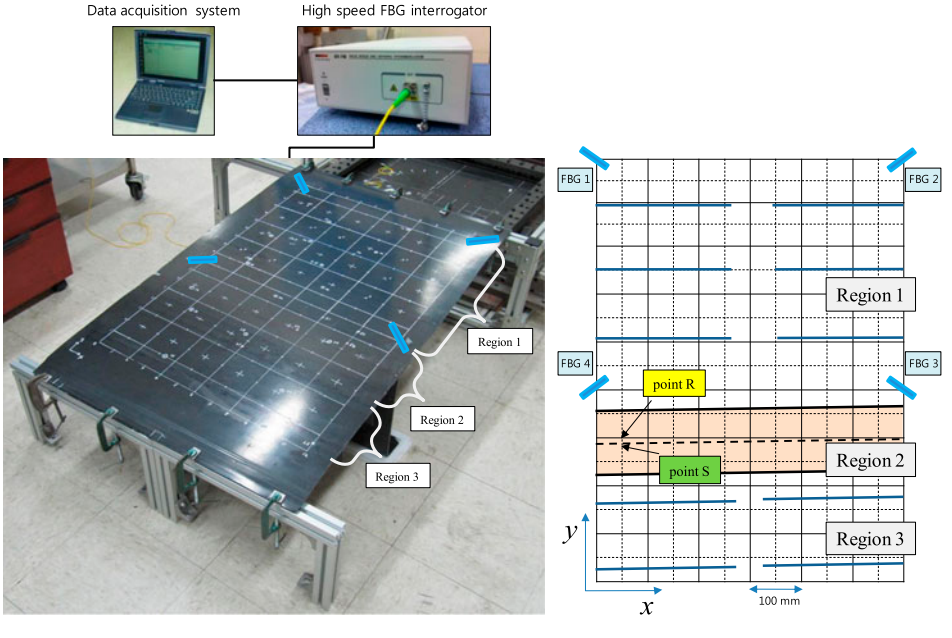

Figure 1. Experimental setup and configuration of the test specimen.

impact hammer. Thus, the impact energies and angles can be slightly different according to each impact event.

A high-speed FBG interrogator is able to capture the wavelength changes of FBG sensors with a sampling frequency of 100 kHz. This interrogator is composed of a superluminescent laser diode, spectrometer, photodiode (PD) array, and readout circuits.[22] The lights reflected by FBG sensors are dispersed in a spectrometer, and converted to electrical signals by the PD array. Electrical signals are then quickly processed by fully parallel readout circuits. From this procedure, this interrogator shows better performance in terms of multiplexing and sampling speed compared to other high-speed FBG interrogators available on the current market.

2.2. *Construction of database*

FBG sensor signals were acquired and saved from the impact experiments about all training points for the database construction. The data was sampled for 55 ms at 100 kHz (5500 data points) in each FBG signal. The (a), (b), and (c) in Figure 2 show one of the signals in each region, respectively. These signals have different features according to their regions. In Region 1, the thickness is smaller and the sensor sensitivity is higher than those of the other regions. Thus, the magnitudes of flexural modes in each FBG signal of Figure 2(a) are relatively higher, and fluctuations are clearly observed. On the other hand, as shown in Figure 2(b), the extensional and flexural

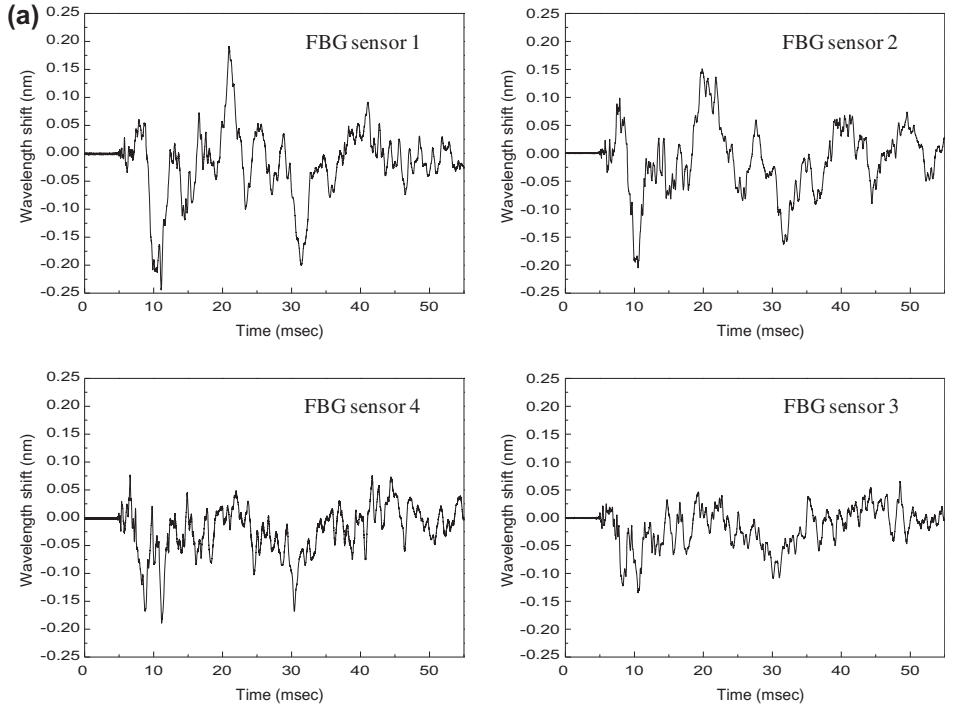

Figure 2. FBG sensor signals in different regions. (a) FBG signals from impact on (0.3, 0.6) – Region 1. (b) FBG signals from impact on (0.3, 0.3) – Region 2. (c) FBG signals from impact on (0.3, 0.1) – Region 3.

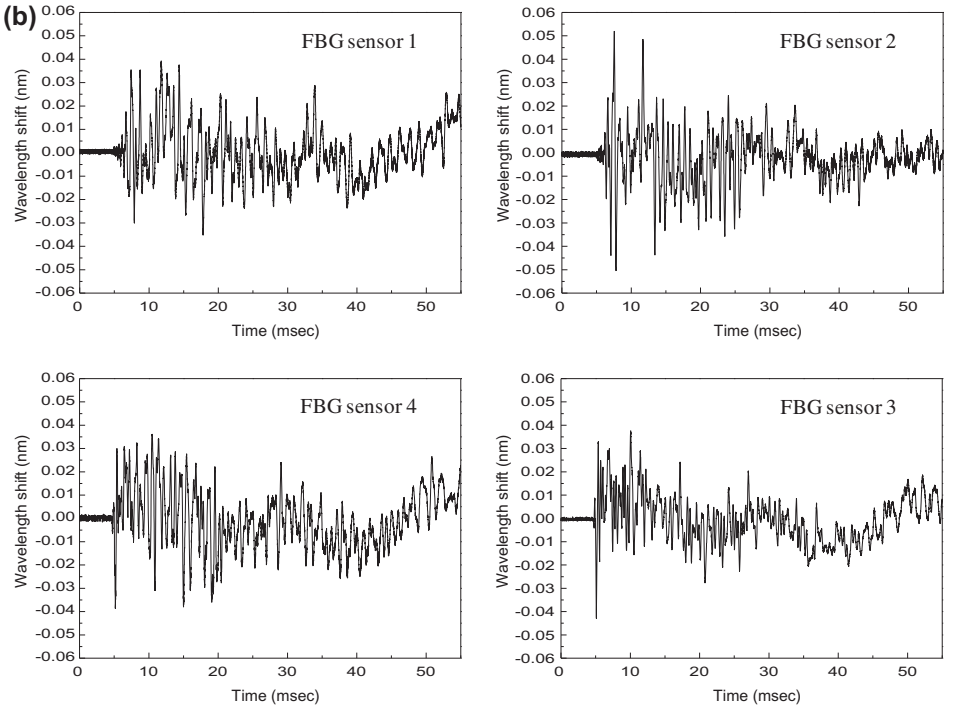

Figure 2. (*Continued*)

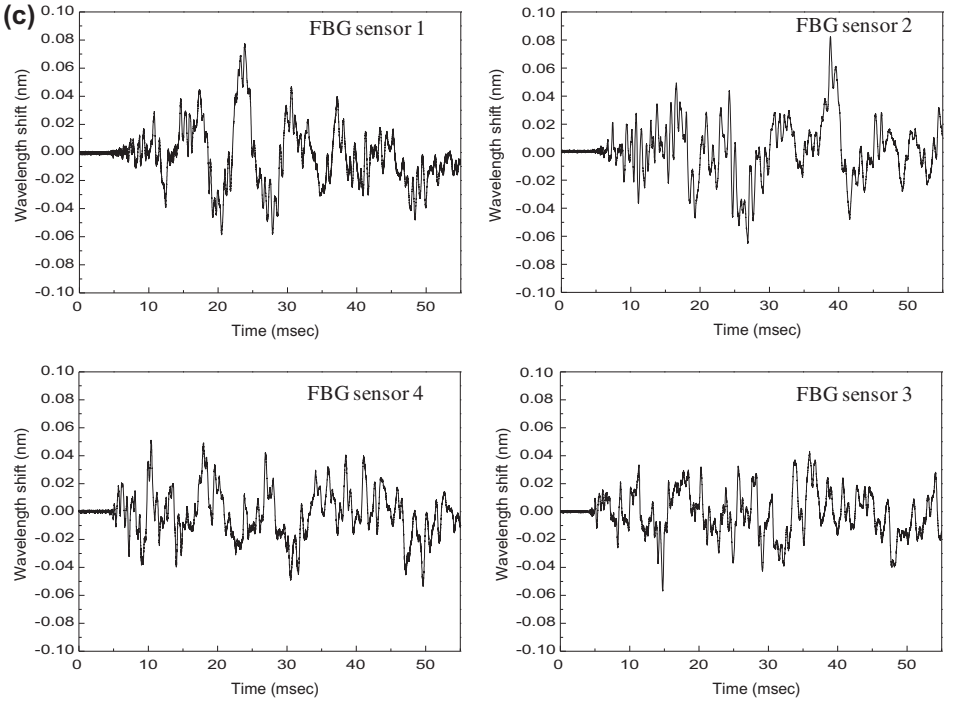

Figure 2. (*Continued*)

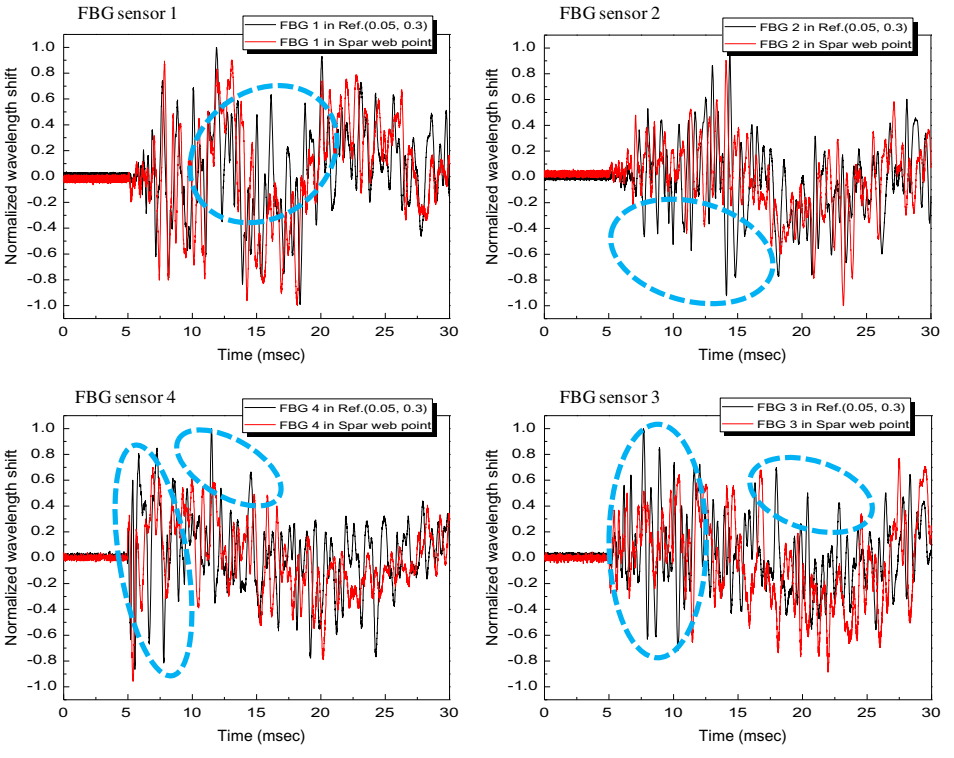

Figure 3. FBG signals at the points R and S.

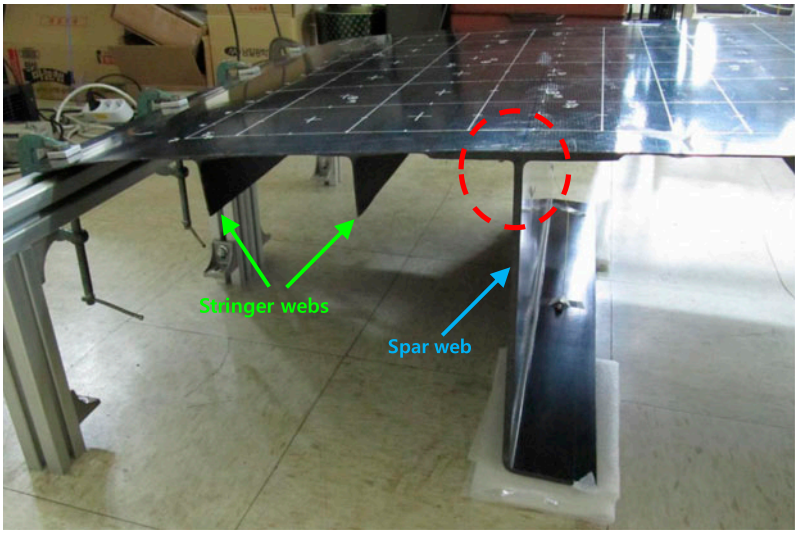

Figure 4. Spar and stringer web positions in Regions 2 and 3.

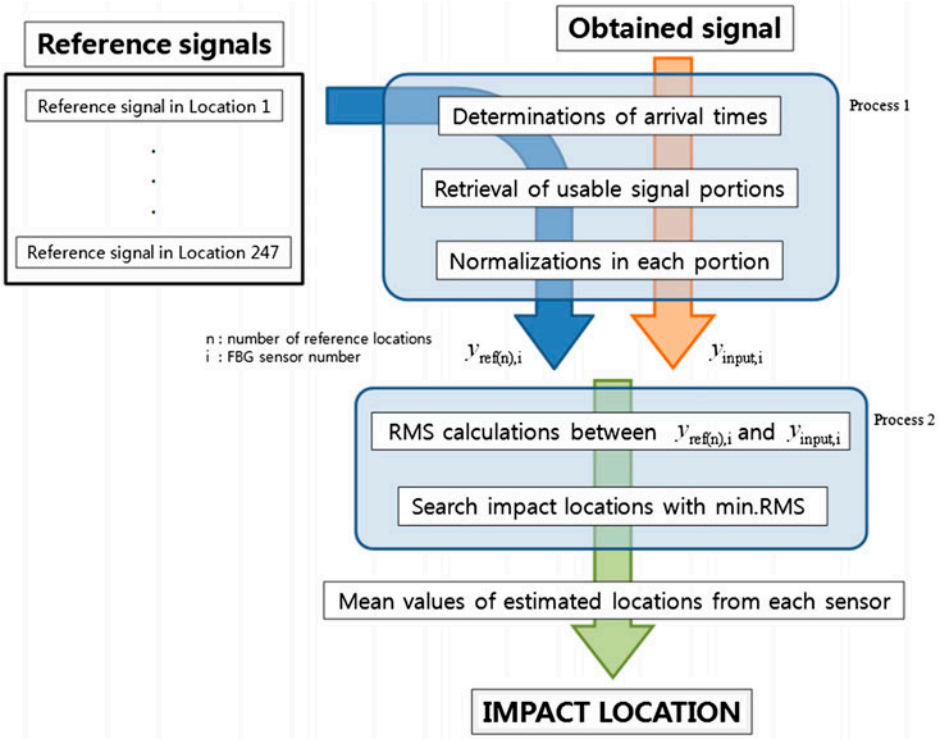

Figure 5. Flow chart for the impact localization algorithm.

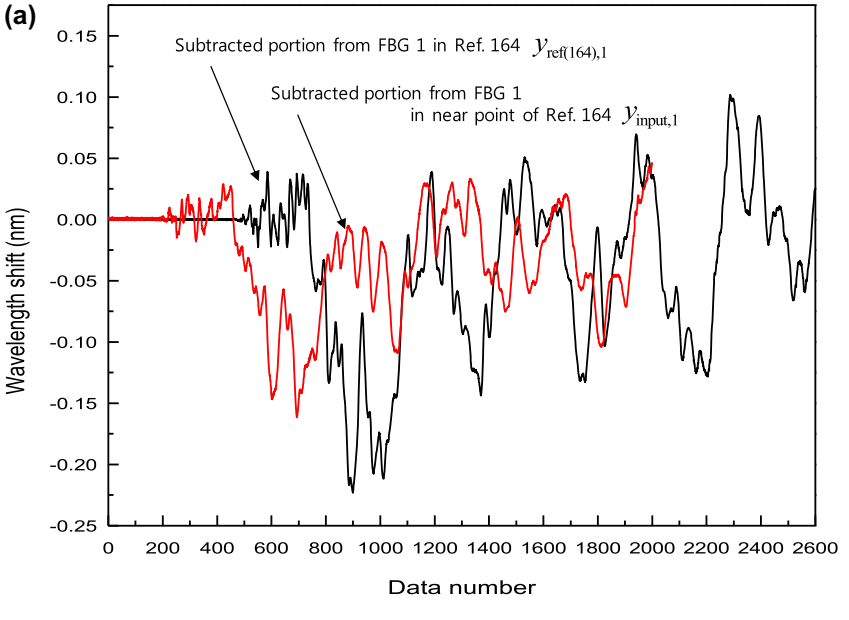

Figure 6. Comparison between the obtained and reference signal. (a) Inappropriate comparison. (b) Appropriate comparison by shifting obtained signal.

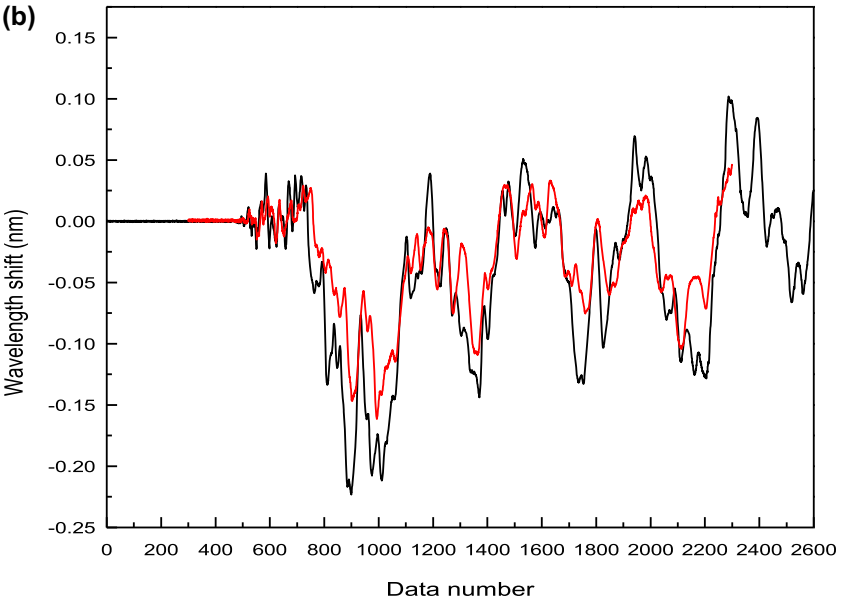

Figure 6. (*Continued*)

modes are not easily distinguished in the signals of Region 2. In other words, the overall magnitudes are decreased and high-frequency portions are increased (the extensional modes are relatively dominant), because this region is the thickest part due to the intermediate spar. Although this region is closer to the sensor locations than is Region 3, the overall magnitudes are similar to those of sensor signals in Region 3. In the case of Region 3, the impact signals were attenuated as shown in Figure 2(c) until they arrived at each sensor due to the long distance and the bonding region between the spar and the skin. These features are commonly observed in the obtained signals in each region.

In addition, the effects of the stiffeners on the impact signals have to be considered for selecting the training points. In order to investigate such effects, the signals of reference point (point R, (0.05, 0.30)) and neighboring point (point S, which is on the spar web position) are plotted in Figure 3. These signals are normalized by each maximum value for comparison. Although these points are located close together, the features of each signal are somewhat different. The overall behaviors are similar to each other, but several high peaks in the neighboring reference signal (indicated by broken-lined circles) appear to be dissipated in the signals of point S. This phenomenon is caused by the structural differences of each point. As Figure 4 indicates, the point S is on top of the spar web position, while the neighboring reference point R is on the spar flange region. Thus, some portion of impact waves was dispersed to the spar web. Due to this reason, high peaks disappeared in the signals of point S. This can induce inaccuracy of the impact localization results. In order to address this problem, the impact signals on the stiffener positions must be included in the database. This means that such structurally discontinuous regions have to be requisitely considered as reference points. As shown in Figure 1, the reference points in Region 1 almost accord with the positions of stringers. However, there are relatively larger deviations in Regions 2 and 3. Thus, additional training signals on these regions must be included to the database as reference signals.

From the low-velocity impact experiments, a database for impact localizations was constructed using the FBG signals from impacts in overall regions. Although there are high attenuation and low sensitivity regions due to different distances and the sensors' directivities, the impact events were appropriately detected in the overall test sections. Thus, impact localization was attempted in all regions, including the regions not surrounded by a sensor network.

3. Impact localization algorithm

The impact localization algorithm proposed in this paper is illustrated in Figure 5. This algorithm is composed of two main processes: Process 1 and 2. First, usable signal portions are retrieved from an obtained signal and all reference signals by Process 1. The starting point of retrieval is determined from the arrival time of each signal. The length of usable data portions (l_o) from an obtained signal was determined as 2000 (20 ms). The length of retrieved portions (l_r) from the reference signals is longer than l_o $(l_r = l_o + 600)$, because the root mean-squared (RMS) value of the difference between the obtained and the reference signals can be improperly calculated due to erroneous arrival time determination. For instance, as shown in Figure 6(a), although an input signal is obtained from a location near one reference point, the RMS value of the difference between two signals can be larger due to the incorrect comparison. Thus, in order to avoid this situation, the RMS values of the difference are calculated and recorded between the reference signals and shifted input signals, and the minimum value is then chosen as the RMS value in that the reference location is as shown in Figure 6(b). This procedure is performed in Process 2.

From Processes 1 and 2, RMS value data of the difference between the obtained signals and all reference signals are acquired for each FBG signal. The reference locations that have the lowest RMS values are searched in each FBG signal. Finally, the impact location is determined as the mean values of x- and y-coordinates in the searched locations from each FBG signal.

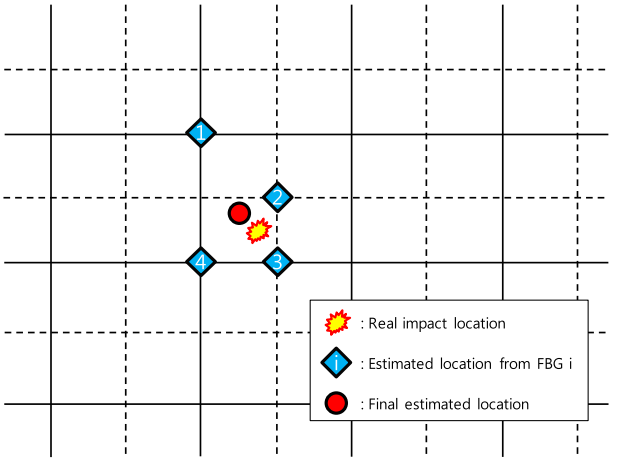

Figure 7. Determination of impact location by averaging estimated locations from each sensor.

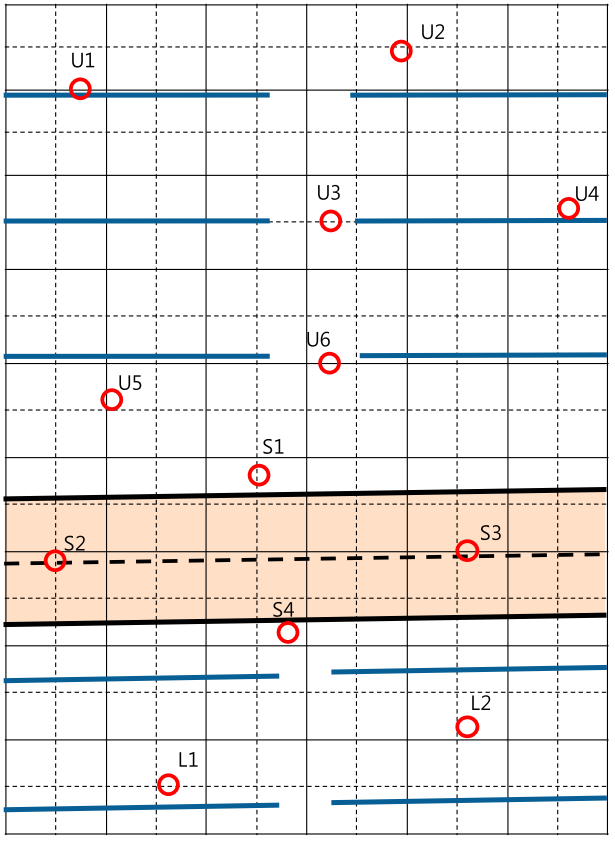

Figure 8. Locations of validation points in the test section.

Table 1. Locations of validation points.

Validation points		Baseline	
		x (m)	y (m)
Region 1	U1	0.0750	0.8000
	U2	0.3920	0.8420
	U3	0.3250	0.6500
	U4	0.5580	0.6630
	U5	0.1060	0.4570
	U6	0.3250	0.5000
Region 2	S1	0.2530	0.3800
	S2	0.0500	0.2860
	S3	0.4630	0.3050
	S4	0.2800	0.2170
Region 3	L1	0.1680	0.0500
	L2	0.4610	0.1100

This algorithm is based on the similarities between an obtained signal and a neighboring reference signal in the database. Thus, a datum point has to be correctly determined for proper comparison. A datum point is determined from the arrival time of the leading wave to a sensor. However, correct determination of the arrival time is quite difficult due to unexpected noise peaks, signal attenuations, and so on. Due to these reasons, this algorithm adopts Process 2, which offers a proper RMS value among the calculated RMS values between a reference signal and shifted obtained signals. By adopting this process, the performance of impact localization is enhanced, and incorrect estimation is substantially reduced.

Moreover, this algorithm estimates the impact location by averaging the locations determined from each sensor. As the diamond-shaped points in Figure 7, impact locations are estimated on the reference points from each FBG signal. Thus, in the case of an arbitrary impact on any point other than the trained reference point, there is an inherent error in the estimated result. In order to resolve this limitation, the mean point of each estimated location is used for the resultant location of the impact. From this procedure, the proposed algorithm in this paper offers an estimated location for the region covered by the sensors as well as other regions with the possibility of increased accuracy.

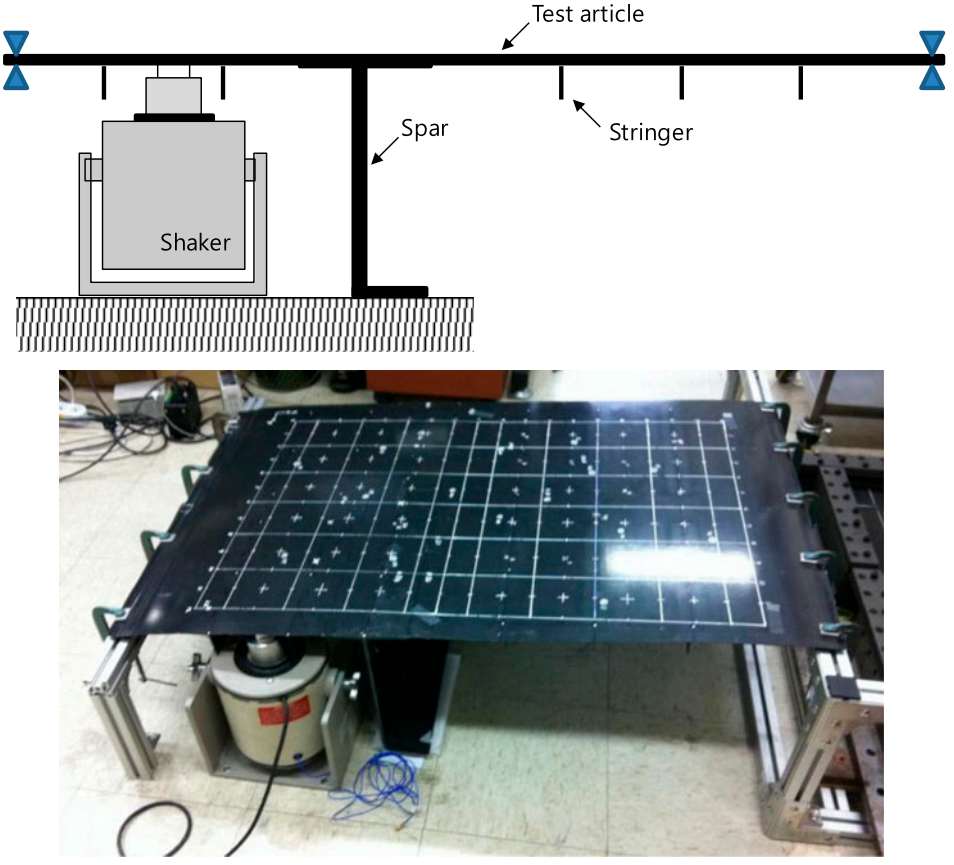

Figure 9. Experimental setup for the validation tests.

4. Validation tests

4.1. Experimental setup for validation tests

In order to validate the proposed impact localization algorithm, validation tests were performed under dynamic loading condition. The locations of the validation points are shown in Figure 8 and listed in Table 1. The total number of validation points is 12, and each point is located in the non-reference regions. There are six points in Region 1, four points in Region 2, and two points in Region 3.

The composite-stiffened panel was excited at the one position in Region 3 using an electrodynamic vibration shaker for simulating the dynamic loading condition, as illustrated in Figure 9. A sine signal with different excitation frequencies (10, 20, and 30 Hz) was adopted as an input function, and the applied excitation amplitude was 9 mm. Compared to the frequency ranges of impact wave (order of kHz), those of external dynamic loadings (order of Hz) are much lower. Thus, such excitation frequency levels were determined. Under dynamic loading conditions with each excitation frequency, impact experiments were performed on the validation points.

As shown in Figure 10, the impact signals were severely affected by the excited dynamic loadings. Such induced differences could sufficiently disturb the impact localization algorithms which use arrival times of the impact waves. Thus, various external environments have to be considered for verifying *in situ* impact localization algorithms. In this study, the dynamic loading condition was considered as the one factor of external environments.

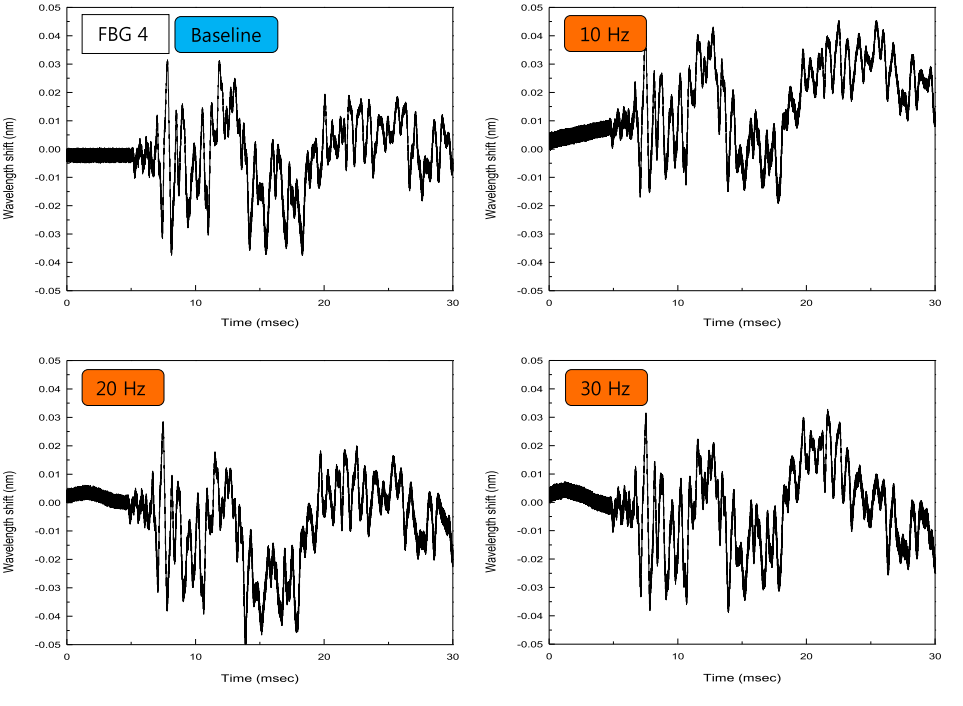

Figure 10. Impact signals on the point S2 under dynamic loading conditions.

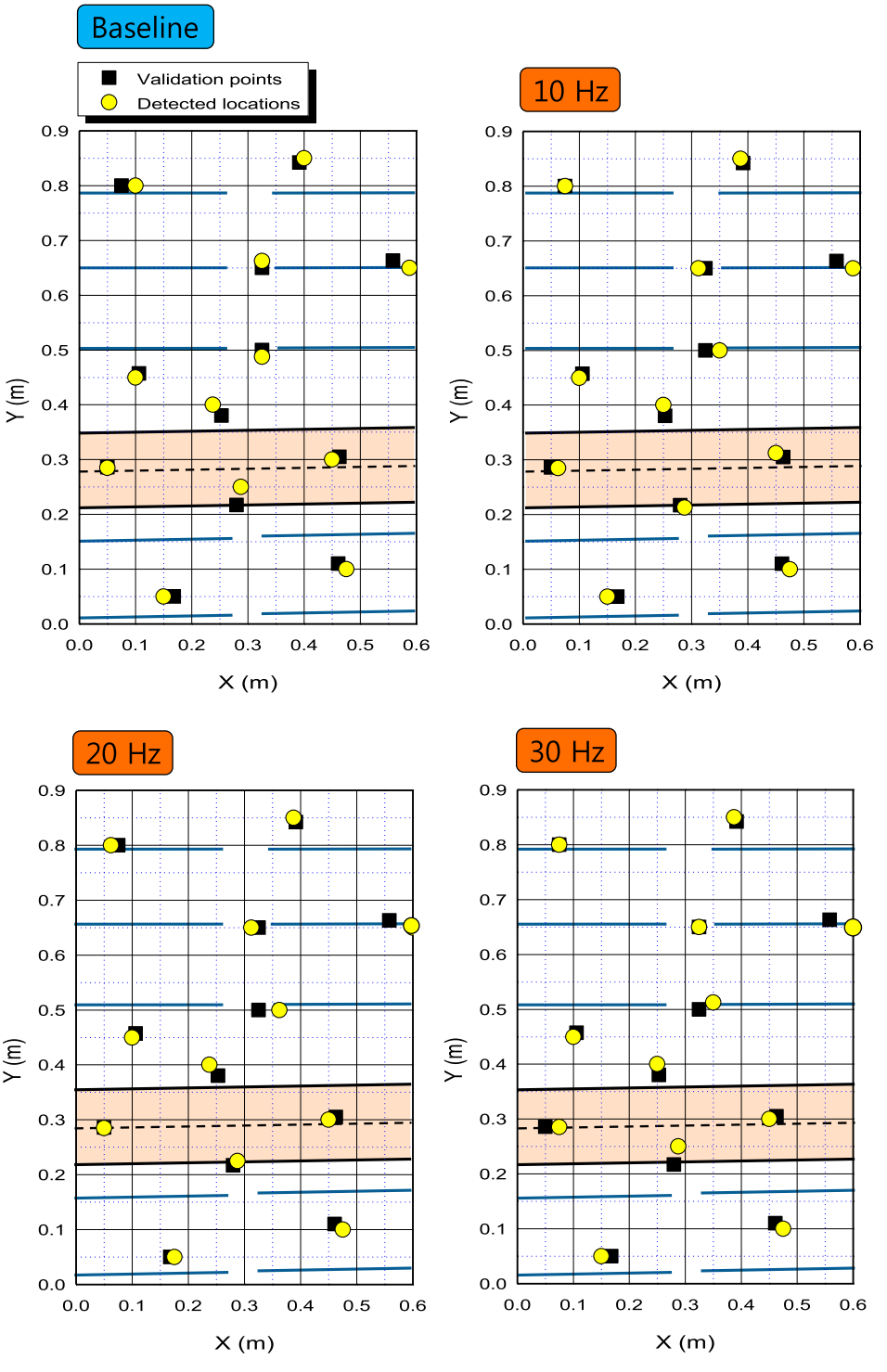

Figure 11. Impact localization results of the validation tests.

Table 2. Detected locations of validation points under dynamic loading conditions.

Validation points		Baseline		Dynamic loading conditions: 10 Hz		20 Hz		30 Hz	
		x (m)	y (m)	x (m)	y (m)	x (m)	y (m)	x (m)	y (m)
Region 1	U1	0.1000	0.8000	0.0750	0.8000	0.0625	0.8000	0.0750	0.8000
	U2	0.4000	0.8500	0.3875	0.8500	0.3875	0.8500	0.3875	0.8500
	U3	0.3250	0.6625	0.3125	0.6500	0.3125	0.6500	0.3250	0.6500
	U4	0.5875	0.6500	0.5875	0.6500	0.6000	0.6500	0.6000	0.6500
	U5	0.1000	0.4500	0.1000	0.4500	0.1000	0.4500	0.1000	0.4500
	U6	0.3250	0.4875	0.3500	0.5000	0.3625	0.5000	0.3500	0.5125
Region 2	S1	0.2375	0.4000	0.2500	0.4000	0.2375	0.4000	0.2500	0.4000
	S2	0.0500	0.2850	0.0625	0.2850	0.0500	0.2850	0.0750	0.2852
	S3	0.4500	0.3000	0.4500	0.3125	0.4500	0.3000	0.4500	0.3000
	S4	0.2875	0.2000	0.2875	0.2125	0.2875	0.2250	0.2875	0.2500
Region 3	L1	0.1500	0.0500	0.1500	0.0500	0.1750	0.0500	0.1500	0.0500
	L2	0.4750	0.1000	0.4750	0.1000	0.4750	0.1000	0.4750	0.1000
Ave. error (m)		0.0177		0.0150		0.0167		0.0182	
Max. error (m)		0.0338		0.0322		0.0440		0.0440	

4.2. *Results*

As previously mentioned, the reference signals in the database were obtained in the baseline condition. The results of the validation tests are shown in Figure 11 and listed in Table 2. In spite of the disturbances by external dynamic loadings, the validation points in all loading conditions showed good results with reasonable accuracy. In addition, the average and maximum errors in the baseline and dynamic loading conditions are almost similar. It means that the comparisons between the reference signals and obtained signals could be correctly performed although the obtained signals were affected by the external dynamic loadings as shown in Figure 10. Also, the validation points in the outside sensor-covered regions were appropriately identified. These results showed that impact events on larger areas can be monitored by the proposed algorithm in this study.

In summary, from the results of validation tests, the performance of the proposed algorithm could be experimentally verified in terms of the accuracy as well as the covered area under external dynamic loading conditions.

5. Conclusion

In this study, a new impact localization algorithm using reference signals was suggested and verified. Four FBG sensors in a single optical fiber line were used to acquire impact-induced AE signals. Impact signals were gathered with a sampling frequency of 100 kHz. The test article was a composite-stiffened panel with a spar and stringers.

The suggested algorithm exploits the similarities between the obtained signal and reference signals. In order to evaluate the similarities, the RMS values were calculated and compared. First, the impact locations were estimated from each sensor signal, and then the final location was determined as the mean value of each estimated location. Through this procedure, the accuracy of impact localization was enhanced.

In order to assess the performance of this algorithm, validation tests were performed on 12 points that were not located at reference grid points under dynamic loading conditions. The results show that the proposed algorithm could successively estimate the validation points in not only the regions covered by sensor but also outside regions in all dynamic loading conditions. From these results, the robustness of the proposed algorithm could be experimentally investigated under external dynamic loading conditions. Also, it can be concluded that this algorithm can cover large areas of a complex composite structure with a small number of sensors. Although the number of reference points and the data size of usable portions need to be studied further, the proposed algorithm can be useful for *in situ* impact monitoring systems.

Acknowledgments

The authors acknowledge supports from the Agency for Defense Development in Korea [contract number UC080019JD]; a grant [07-02] from the Aviation Safety R&D Program funded by the Ministry of Land, Transport and Maritime Affairs of the Korean government; and Nuclear Research and Development Program [grant number 2011-0019198] through the National Research Foundation of Korea funded by the Ministry of Education, Science and Technology.

References

[1] Greene JA, Tran TA, Bhatia V, Gunther MF, Wang A, Murphy KA, Claus RO. Optical fiber sensing technique for impact detection and location in composites and metal specimens. Smart Mater. Struct. 1995;4:93–99.
[2] Sekine H, Atobe S. Identification of locations and force histories of multiple point impacts on composite isogrid-stiffened panels. Compos. Struct. 2009;89:1–7.
[3] Park SO, Jang BW, Lee YG, Kim YY, Kim CG, Park CY, Lee BW. Detection of impact location for composite stiffened panel using FBG sensors. Adv. Mater. Res. 2010; 123–125:895–898.
[4] Jang BW, Lee YG, Kim JH, Kim YY, Kim CG. Real-time impact identification algorithm for composite structures using fiber Bragg grating sensors. Struct. Control Health Monit. 2012;19:580–591.
[5] Jang BW, Park SO, Lee YG, Kim CG, Park CY. Detection of impact damage in composite structures using high speed FBG interrogator. Adv. Compos. Mater. 2012;21:29–44.
[6] Gaul L, Hurlebaus S. Identification of the impact location on a plate using wavelets. Mech. Syst. Signal Process. 1998;12:783–795.
[7] Sung DU, Oh JH, Kim CG, Hong CS. Impact monitoring of smart composite laminates using neural network and wavelet analysis. J. Intell. Mater. Syst. Struct. 2000;11:180–190.
[8] Seydel R, Chang FK. Impact identification of stiffened composite panels: I. System development. Smart Mater. Struct. 2001;10:354–369.
[9] Seydel R, Chang FK. Impact identification of stiffened composite panels: II. Implementation studies. Smart Mater. Struct. 2001;10:370–379.
[10] Coverley PT, Staszewski WJ. Impact damage location in composite structures using optimized sensor triangulation procedure. Smart Mater. Struct. 2003;12:795–803.
[11] Meo M, Zumpano G, Piggott M, Marengo G. Impact identification on a sandwich plate from wave propagation responses. Compos. Struct. 2005;71:302–306.
[12] LeClerc JR, Worden K, Staszewski WJ. Impact detection in an aircraft composite panel – a neural-network approach. J. Sound Vib. 2007;299:672–682.
[13] Ciampa F, Meo M. A new algorithm for acoustic emission localization and flexural group velocity determination in anisotropic structures. Composites Part A. 2010;41:1777–1786.
[14] Baxter MG, Pullin R, Holford KM, Evans SL. Delta T source location for acoustic emission. Mech. Syst. Signal Process. 2007;21:1512–1520.
[15] Kundu T, Das S, Martin SA, Jata KV. Locating point of impact in anisotropic fiber reinforced composite plates. Ultrasonics. 2008;48:193–201.

[16] Hajzargerbashi T, Kundu T, Bland S. An improved algorithm for detecting point of impact in anisotropic inhomogeneous plates. Ultrasonics. 2011;51:317–324.
[17] Ing RK, Quieffin N, Catheline S, Fink M. In solid localization of finger impacts using acoustic time-reversal process. Appl. Phys. Lett. 2005;87:204104-1–204104-3.
[18] Ribay G, Catherline S, Clorennec D, Ing RK, Quieffin N, Fink M. Acoustic impact localization in plates: properties and stability to temperature variation. IEEE Trans. Ultrason. Ferroelectr. Freq. Control. 2007;54:373–385.
[19] Chen C, Yuan FG. Impact source identification in finite isotropic plates using a time-reversal method: theoretical study. Smart Mater. Struct. 2010;19:105028(11p).
[20] Chen C, Li Y, Yuan FG. Development of time-reversal method for impact source identification on plate structures. Shock Vib. 2013;20:561–573.
[21] Ciampa F, Meo M, Barbieri E. Impact localization in composite structures of arbitrary cross section. Struct. Health Monit. 2012;11:643–655.
[22] Polimeno U, Meo M, Almond DP, Angioni SL. Detecting low velocity impact damage in composite plate using nonlinear acoustic/ultrasound methods. Appl. Compos. Mater. 2010;17:481–488.
[23] Aymerich F, Staszewski WJ. Experimental study of impact-damage detection in composite laminates using a cross-modulation vibro-acoustic technique. Struct. Health Monit. 2010;9:541–553.
[24] Ciang CC, Lee JR, Bang HJ. Structural health monitoring for a wind turbine system: a review of damage detection methods. Meas. Sci. Technol. 2008;19:1–20.
[25] Lee JS, Park GH, Kim CG, Farrar CR. Use of relative baseline features of guided waves for *in situ* structural health monitoring. J. Intell. Mater. Syst. Struct. 2011;22:175–189.
[26] Betz DC, Thursby G, Culshaw B, Staszewski WJ. Acousto-ultrasonic sensing using fiber Bragg gratings. Smart Mater. Struct. 2003;12:122–128.
[27] Lee JR, Lee SS, Yoon DJ. Simultaneous multipoint acoustic emission sensing using fibre acoustic wave grating sensors with identical spectrum. J. Opt. A: Pure Appl. Opt. 2008;10:085307-9.
[28] Lee JR, Chong SY, Yun CY, Yoon DJ. A lasing wavelength stabilized simultaneous multipoint acoustic sensing system using pressure-coupled fiber Bragg gratings. Opt. Lasers Eng. 2011;49:110–120.
[29] Lee BW, Seo MS, Oh HG, Park CY. High-speed wavelength interrogator of fiber Bragg gratings for capturing impulsive strain waveforms. Adv. Mater. Res. 2010;123–125: 867–870.